ChemComm

COMMUNICATION

View Article Online
View Journal | View Issue

Cite this: *Chem. Commun.*, 2026, **62**, 3531

Received 13th December 2025,
Accepted 9th January 2026

DOI: 10.1039/d5cc07080e

rsc.li/chemcomm

A fluorescent conjugated polymer-based ratiometric aptasensor for highly specific and robust detection of perfluorooctanoic acid

Hao Liu,[a] Qin-feng Xu, *[a] Zhao-zhao Zhang,[a] Yan-ni Li[a] and Chun-yang Zhang *[b]

We develop a fluorescent conjugated polymer-based ratiometric aptasensor for highly specific and robust detection of perfluorooctanoic acid (PFOA). The presence of PFOA can induce aptamer folding and consequently the enhancement of the fluorescence resonance energy transfer (FRET) efficiency, facilitating the ratiometric detection of PFOA with a detection limit of 27 nM and excellent selectivity. This robust aptasensor can discriminate PFOA from common anionic surfactants, which remains a challenge for conjugated polymer–based PFOA sensors, and visually measures PFOA in complex aqueous samples.

Perfluorinated and polyfluorinated alkyl substances (PFAS) are synthetic organic pollutants widely used in food packaging and fire-fighting foams.[1] Their extensive use has led to widespread contamination of surface and groundwater. Human exposure to PFAS may induce carcinogenicity, reproductive and endocrine disruption, neurotoxicity, dyslipidaemia, and immunotoxicity.[1,2] Among PFAS, perfluorooctanoic acid (PFOA) is of particular importance, because it has been detected in the majority of serum samples from the exposed populations worldwide, with water being identified as the primary route of exposure.[3]

Liquid chromatography-mass spectrometry (LC-MS) is currently the standard technique for detecting PFOA with good performance.[4] However, it requires expensive instrumentation, skilled operation, and time-consuming procedures. Therefore, alternative methods for rapid, portable, and cost-effective detection of PFOA are highly desirable. So far, a variety of fluorescence-based platforms based on metal–organic cages,[5] covalent organic frameworks,[6] macrocycles,[7] metal–organic frameworks,[8] metal complexes,[9] and other materials[10] have been reported for PFAS analysis. Nevertheless, most of these methods rely on single-emission intensity measurement, making them vulnerable to instrumental fluctuations and environmental interference.[11] In contrast, ratiometric fluorescent methods can monitor analyte-induced changes at two (or more) emission bands, providing an internally self-calibrated signal that significantly minimizes environmental interference and reduces measurement ambiguity.[11] Although ratiometric strategies have gained increasing attention, their application to PFAS detection is rare. Recently, fluorescent conjugated polymers (FCPs) have been reported for ratiometric fluorescence sensing of PFAS due to their strong light-harvesting capability and high sensitivity.[12] Unfortunately, these FCP-based methods suffer from the interference caused by anionic surfactants commonly present in natural water systems, which significantly hampers their practical applications.[12,13] To overcome this issue, the development of robust methods capable of selectively recognizing PFAS against surfactant interferents is necessary.

The integration of DNA aptamers into fluorescence sensing systems can improve the assay specificity.[14] Aptamers are single-stranded DNA (ssDNA) or RNA molecules that undergo three-dimensional conformational changes upon binding to their targets, and they exhibit high affinity and good specificity.[15] When the positively charged FCPs are combined with the negatively charged DNA, highly efficient fluorescence resonance energy transfer (FRET) can be achieved with the FCPs acting as the energy donors and the dye labels attached to the oligonucleotide terminus acting as the energy acceptors.[16] The further integration of aptamers with FCPs may generate the target-specific fluorescence response.[17] Since the discovery of a PFOA-binding aptamer by Park in 2022, this aptamer has been widely applied for specific detection of PFOA.[14,18] Herein, we develop a conjugated polymer-based ratiometric aptasensor for highly specific and robust detection of PFOA. This aptamer-regulated ratiometric aptasensor can effectively suppress the interference from common anionic surfactants and overcome the prevalent selectivity challenge in conventional PFOA sensors. The sensing mechanism is illustrated in Scheme 1.

[a] *School of Food Science and Engineering, Shaanxi University of Science and Technology, Xi'an, Shaanxi 710021, P. R. China. E-mail: xuqinfeng@sust.edu.cn*
[b] *School of Chemistry and Chemical Engineering, Southeast University, Nanjing, 211189, P. R. China. E-mail: zhangcy@seu.edu.cn*

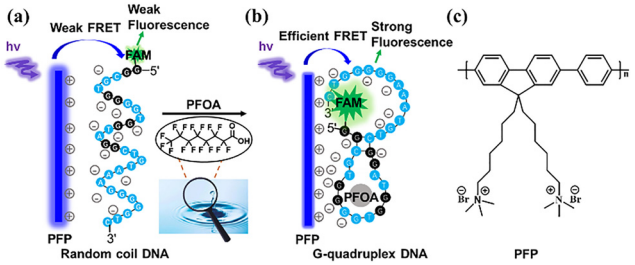

Scheme 1 (a) and (b) Schematic illustration of a fluorescent conjugated polymer-based ratiometric aptasensor for sensitive detection of PFOA. (c) Chemical structure of the cationic polyfluorene (PFP).

A PFOA aptamer labeled with 5′-terminal fluorescein (Apt-FAM) is employed as the recognition element. In the absence of PFOA, the ssDNA adopts a random coil conformation,[14] resulting in a weak electrostatic interaction with the FCP.[19] As a result, the fluorophore remains spatially distant from the FCP, and no significant FRET-based signal is observed (Scheme 1a).[19] Upon the addition of PFOA, the aptamer folds into a compact G-quadruplex structure,[14] which increases the local negative charge density and significantly enhances electrostatic attraction toward the cationic FCP.[19] Such structural transformation brings the FCP into close proximity with the fluorophore, generating a FRET-based signal (Scheme 1b).[19] Poly (9,9-bis (6′-*N*,*N*,*N*-trimethylammonium) hexyl) fluorenylene phenylene (PFP) is employed as the FCP donor (Scheme 1c). FAM is selected as the acceptor fluorophore, because its excitation spectrum overlaps with the emission of PFP (Fig. 1a). Upon excitation at 380 nm, PFP is selectively excited to produce a FRET-based ratiometric fluorescence response.[20]

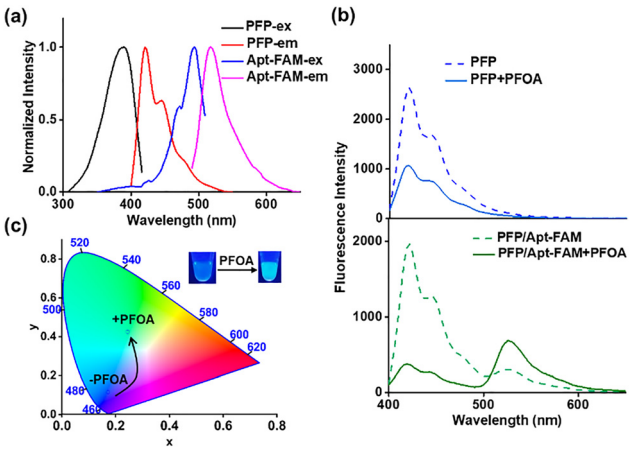

Fig. 1 Feasibility validation of the proposed conjugated polymer–based aptamer-regulated ratiometric aptasensor for PFOA detection. (a) Normalized fluorescence excitation spectra of PFP (black) and Apt-FAM (blue), and fluorescence emission spectra of PFP (red) and Apt-FAM (pink). (b) Emission spectra of PFP (blue) and the PFP/Apt-FAM system (green) in the absence (dotted line) and presence of PFOA (solid line). λ_{ex} = 380 nm, [PFOA] = 30 μM, [ssDNA-FAM] = 25 nM, [PFP] = 2.5 μM. Measurements were performed in HEPES buffer (20 mM HEPES, 1 mM NaCl, pH 7.4). (c) CIE chromaticity coordinates of PFP/Apt-FAM fluorescence before and after the addition of PFOA. Inset: photographs of the PFP/Apt-FAM solution in the absence (left part) and presence (right part) of PFOA under 385-nm UV irradiation.

As shown in Fig. 1b, PFP alone exhibits a distinct fluorescence emission at 420 nm, but it decreases by approximately 2.5-fold upon the addition of PFOA. In the presence of both PFP and Apt-FAM, dual fluorescence signals at 420 nm (PFP) and 525 nm (FAM) are observed. Upon the addition of PFOA, the FRET ratio (I_{525}/I_{420}) increases by nearly 11.7-fold, suggesting that the incorporation of Apt-FAM can convert the system from a signal-off mode to a ratiometric mode. To visualize this change, we calculated the Commission Internationale de l'Éclairage (CIE) chromaticity coordinates from the fluorescence spectra.[21] After the addition of PFOA, the coordinates shift from blue (0.172, 0.115) to green (0.245, 0.425) (Fig. 1c). A corresponding blue-to-green transition is directly observed under 385 nm UV illumination (Fig. 1c, inset). Theoretically, the total color change (ΔE^*) value above 2 is generally considered perceptible to the observer.[22] The ΔE^* between the PFP/Apt-FAM solutions with and without PFOA reaches 81.51, indicating an exceptionally prominent and easily distinguishable color change. These results demonstrate that PFOA can be detected by not only the ratiometric FRET signal (I_{525}/I_{420}) but also the straightforward visual inspection under UV light.

To quantitatively evaluate PFOA, we recorded the fluorescence intensities at various PFOA concentrations under the optimized experimental conditions (Fig. S1–S3). As shown in Fig. 2a, upon excitation at 380 nm, the FRET ratio (I_{525}/I_{420}) increases progressively with increasing PFOA concentration. A good linear correlation is obtained between the $(I_{525}/I_{420})/(I_{525}/I_{420})_0$ value and the PFOA concentration in the range of 0–30 μM (Fig. 2b). The resulting linear regression equation is $(I_{525}/I_{420})/(I_{525}/I_{420})_0 = 0.359 \times [\text{PFOA}] + 1$ ($R^2 = 0.995$), where (I_{525}/I_{420}) and $(I_{525}/I_{420})_0$ denote the FRET ratios measured in the presence and absence of PFOA, respectively. The limit of detection (LOD) is calculated to be 27 nM based on the $3\sigma/k$ method, in which σ represents the standard deviation of the *y*-intercepts of the regression line and k is the slope of the calibration curve. The sensitivity of this ratiometric aptasensor is 67.4-fold higher than that of a calixarene–based fluorescent method (1820 nM),[7e] 100-fold higher than that of a multi-head cationic siloxane–based fluorescent method (2700 nM),[10a] and 6.3-fold higher than that of an ssDNA aptamer-based fluorescent method (170 nM)[14b] (Table S1). To further verify the sensitivity enhancement achieved by this ratiometric aptasensor, we conducted the control experiments in the absence of Apt-FAM. As shown in Fig. S4, without Apt-FAM, the fluorescence intensity of PFP is markedly quenched upon the addition of PFOA. The LOD obtained in the presence of Apt-FAM (0.027 μM) is approximately 40-fold lower than that obtained without Apt-FAM (1.1 μM) (Fig. 2b). This significant improvement can be attributed to (1) the enhanced FRET-based signal and (2) the ratiometric measurement of fluorescence signals.[20]

It is noteworthy that the reported limit of detection (27 nM) is not the lowest among the reported PFAS sensors. Some conjugated polymer/carbon dot-based ratiometric sensors for PFOS assay[12a,23] and the aptamer-based amplification sensor

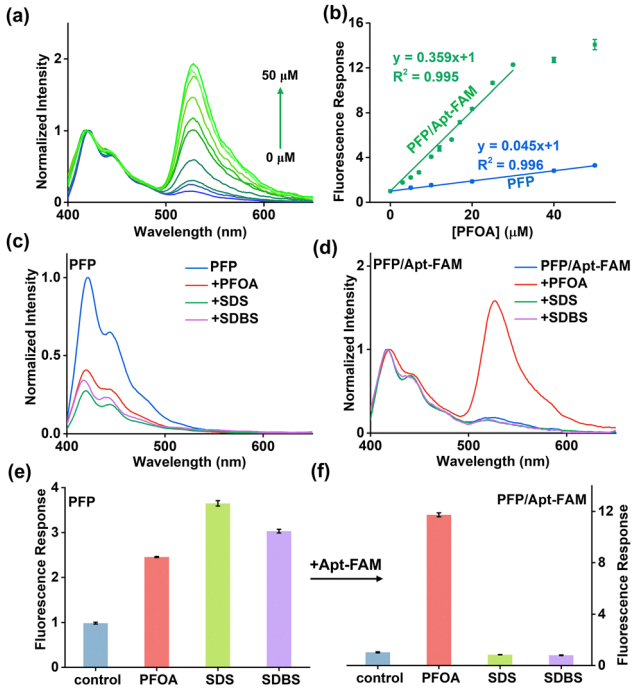

Fig. 2 Contribution of the aptamer to the enhanced sensitivity and selectivity. (a) Emission spectra of the PFP/Apt-FAM system in response to increasing concentrations of PFOA (0–50 μM). (b) Fluorescence response of the PFP/Apt-FAM system (green) and PFP alone (blue) induced by increasing concentrations of PFOA. Emission spectra of PFP (c) and PFP/Apt-FAM (d), and the corresponding fluorescence responses of PFP (e) and PFP/Apt-FAM (f) in the absence (blue) and presence of PFOA (red), SDS (green), and SDBS (purple). [SDS] = [SDBS] = [PFOA]= 30 μM. For PFP alone, fluorescence response = I_0/I. For the PFP/Apt-FAM system, fluorescence response = $(I_{525}/I_{420})/(I_{525}/I_{420})_0$. The error bars represent the standard deviation derived from three independent measurements.

for PFOA assay[18a] can achieve comparable nM-level sensitivity or lower. The key advancement of our system lies in the enhanced selectivity and robustness provided by the ratiometric aptasensor design. We examined the selectivity of this ratiometric aptasensor toward the anionic surfactants sodium dodecyl sulfate (SDS) and sodium dodecylbenzenesulfonate (SDBS) because they are common anionic surfactants in environmental samples with structures similar to PFAS.[13] As shown in Fig. 2c and e, SDS and SDBS induce significant fluorescence quenching in the PFP system alone, similar to the response observed with PFOA. However, once Apt-FAM is introduced, no significant fluorescence response is observed in the presence of SDS and SDBS, but a pronounced fluorescence change is observed in the presence of PFOA (Fig. 2d and f), suggesting that this ratiometric aptasensor can effectively discriminate PFOA from structurally similar surfactants.

To assess the selectivity of this ratiometric aptasensor toward potential environmental interferents, we challenged the PFP/Apt-FAM system with a range of other PFAS including perfluorobutyric acid (PFBA), perfluorobutanesulfonic acid (PFBS), and perfluorohexanoic acid (PFHxA), octanoic acid, (OA, a structural analogue of PFOA), and several common inorganic salts (*i.e.*, $CaCl_2$, $MgCl_2$, KCl, NaCl, and Na_2SO_4). In

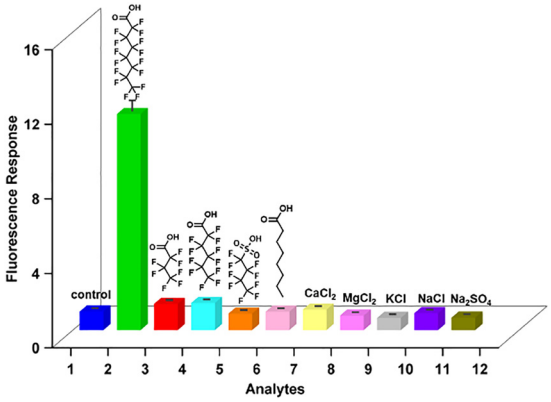

Fig. 3 Evaluation of the selectivity of the sensor toward PFOA against interfering PFAS and inorganic salts. Fluorescence responses of the PFP/Apt-FAM system toward various analytes. λ_{ex} = 380 nm. [Apt-FAM] = 25 nM, [PFP] = 2.5 μM. [PFOA] = [analytes] = 30 μM. 1, control; 2, PFOA; 3, PFBA; 4, PFHxA; 5, PFBS; 6, OA; 7, $CaCl_2$; 8, $MgCl_2$; 9, KCl; 10, NaCl; 11, Na_2SO_4. Fluorescence response = $(I_{525}/I_{420})/(I_{525}/I_{420})_0$. The error bars represent the standard deviation derived from three independent measurements.

all cases, the fluorescence responses remain essentially unchanged (Fig. 3), suggesting that this ratiometric aptasensor is capable of accurately distinguishing PFOA from other potential interferents.

To validate the practical applications of this ratiometric aptasensor, we developed a simple and cost-effective portable device that consists of a sample chamber, an 8-tube strip, and an array of 385-nm LEDs (Fig. 4a). The distinct fluorescence responses of the PFP/Apt-FAM system at varying PFOA concentrations facilitates real-time on-site visual detection of PFOA using a smartphone with the integration of a readily available

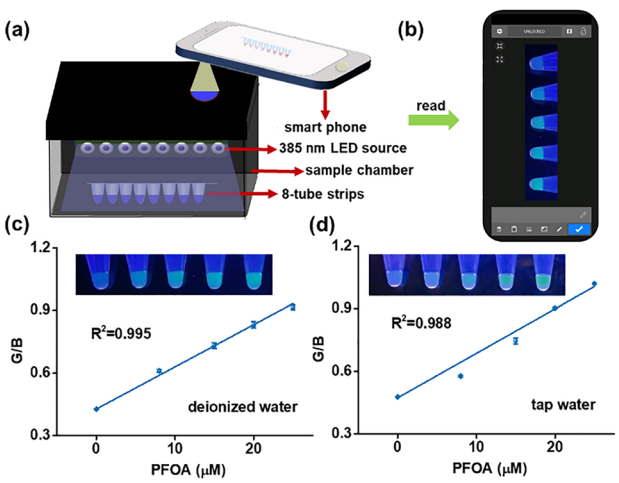

Fig. 4 Design of the portable ratiometric aptasensor for PFOA detection. (a) Blueprint of a visual device designed for quantitative detection of PFOA. (b) Images are recorded by using a smart phone with the color-scanning app Color Grab. Photographs and calibration curves of the PFP/Apt-FAM system in response to different concentrations of PFOA in deionized water (c) and tap water (d). The error bars represent the standard deviation derived from three independent measurements.

color-analysis app (Fig. 4b). Green (G) and blue (B) channel intensities are extracted from the fluorescence images, and the resulting G/B ratios are used to construct a calibration curve with the PFOA concentration (Fig. 4c). To evaluate the performance of this ratiometric aptasensor in real water samples, we spiked various concentrations of PFOA into tap water and measured them with a portable device. As shown in Fig. 4d, under 385-nm UV illumination, the fluorescence color of the solution gradually shifts from blue to green with increasing PFOA concentration, and the G/B ratio extracted from the images exhibits a linear correlation with the PFOA concentration. These results demonstrate the feasibility of this ratiometric aptasensor for rapid, on-site detection of PFOA in complex environmental water samples.

In conclusion, we have developed a fluorescent conjugated polymer-based ratiometric aptasensor for highly specific and robust detection of PFOA with an LOD of 27 nM. This sensing platform offers several distinct advantages: (1) The PFP donor possesses excellent light-harvesting and signal-amplification properties, which greatly enhance the FRET-based signal response. (2) The integration of the PFOA aptamer can transform a simple turn-off response to a self-calibrated ratiometric signal, greatly enhancing the detection accuracy, robustness, and selectivity. This aptasensor not only effectively discriminates PFOA from common anionic surfactant interferents, which remains a challenge for conjugated polymer-based PFOA sensors, but also facilitates rapid and visual detection of PFOA in complex aqueous samples, providing a new paradigm for food safety and environmental monitoring.

This work was financially supported by the National Natural Science Foundation of China (22074085), the Department of Science and Technology of Shaanxi Province (2025CY-JJQ-206), the Education Department of Shaanxi Province (25JC028) and the Department of Human Resources and Social Security of Shaanxi Province (24019).

Conflicts of interest

There are no conflicts to declare.

Data availability

The data supporting this article have been included as part of the supplementary information (SI). Chemicals and materials, experimental procedures, optimization of experimental conditions, emission spectra of the PFP system at increasing concentrations of PFOA, and comparative sensing performance with previously reported sensors are available on SI. See DOI: https://doi.org/10.1039/d5cc07080e.

References

1 M. G. Evich, M. J. B. Davis, J. P. McCord, B. Acrey, J. A. Awkerman, D. R. U. Knappe, A. B. Lindstrom, T. F. Speth, C. Tebes-Stevens, M. J. Strynar, Z. Wang, E. J. Weber, W. M. Henderson and J. W. Washington, *Science*, 2022, **375**, eabg9065.
2 (*a*) X. Zhang, R. Lohmann and E. M. Sunderland, *Environ. Sci. Technol.*, 2019, **53**, 12348–12356; (*b*) M. Ateia, A. Maroli, N. Tharayil and T. Karanfil, *Chemosphere*, 2019, **220**, 866–882.
3 C. Lau, K. Anitole, C. Hodes, D. Lai, A. Pfahles-Hutchens and J. Seed, *Toxicol. Sci.*, 2007, **99**, 366–394.
4 (*a*) K. J. Harris, G. Munoz, V. Woo, S. Sauvé and A. A. Rand, *Environ. Sci. Technol.*, 2022, **56**, 14594–14604; (*b*) E. Olkowska, Ż. Polkowska and J. Namieśnik, *Chem. Rev.*, 2011, **111**, 5667–5700; (*c*) D. Cserbik, P. E. Redondo-Hasselerharm, M. J. Farré, J. Sanchís, A. Bartolomé, A. Paraian, E. M. Herrera, J. Caixach, C. M. Villanueva and C. Flores, *npj Clean Water*, 2023, **6**, 16.
5 Y. He, D. Luo, V. M. Lynch, M. Ahmed, J. L. Sessler and X. Chi, *Chem*, 2023, **9**, 93–101.
6 A. Jrad, G. Das, N. Alkhatib, T. Prakasam, F. Benyettou, S. Varghese, F. Gándara, M. Olson, S. Kirmizialtin and A. Trabolsi, *Nat. Commun.*, 2024, **15**, 10490.
7 (*a*) Z. Chen, Y. L. Lu, L. Wang, J. Xu, J. Zhang, X. Xu, P. Cheng, S. Yang and W. Shi, *J. Am. Chem. Soc.*, 2023, **145**, 260–267; (*b*) R. Lian, Y. D. Yang, J. L. Moreno, Jr., B. L. Eggimann, J. Chen, L. J. Gibson-Elias, C. G. Williams, P. Jiang, A. J. Lee, L. J. Mueller, J. L. Sessler, J. I. Siepmann, D. W. Johnson and R. J. Hooley, *J. Am. Chem. Soc.*, 2025, **147**, 22768–22777; (*c*) S. N. Lei and H. Cong, *Chin. Chem. Lett.*, 2022, **33**, 1493–1496; (*d*) Z. Zheng, H. Yu, W. C. Geng, X. Y. Hu, Y. Y. Wang, Z. Li, Y. Wang and D. S. Guo, *Nat. Commun.*, 2019, **10**, 5762; (*e*) T. Y. Guo, C. L. Duncan, H. W. Li, C. X. Zhang, M. Mocerino and Y. Wu, *Spectrochim. Acta, Part A*, 2023, **302**, 123127.
8 (*a*) H. Q. Yin, K. Tan, S. Jensen, S. J. Teat, S. Ullah, X. Hei, E. Velasco, K. Oyekan, N. Meyer, X. Y. Wang, T. Thonhauser, X. B. Yin and J. Li, *Chem. Sci.*, 2021, **12**, 14189–14197; (*b*) B. Chen, Z. Yang, X. Qu, S. Zheng, D. Yin and H. Fu, *ACS Appl. Mater. Interfaces*, 2021, **13**, 47706–47716; (*c*) Z. Han, Y. Guo, K. Y. Wang, W. Li, J. Huo, Q. Huang, V. I. Bakhmutov, Y. Yang, R. R. Liang, P. R. Taylor, W. Shi and H. C. Zhou, *Angew. Chem., Int. Ed.*, 2025, e15775.
9 (*a*) M. H. Hassan, R. Khan, D. Andreescu, S. Shrestha, M. Cotlet and S. Andreescu, *Adv. Funct. Mater.*, 2024, **34**, 2403364; (*b*) O. Baumeyer, A. Wu, A. Pandya, P. Nelson, P. C. Hillesheim, M. Zeller, G. M. Carignan, J. Li and D. W. Ki, *Chem. Commun.*, 2025, **61**, 10170–10173.
10 (*a*) Z. Gou, A. Wang, X. Zhang, Y. Zuo and W. Lin, *Sens. Actuators, B*, 2022, **367**, 132017; (*b*) Q. Zhang, M. Liao, K. Xiao, K. Zhuang, W. Zheng and Z. Yao, *Sens. Actuators, B*, 2022, **350**, 130851.
11 (*a*) X. Yang, C. Li, P. Li and Q. Fu, *Theranostics*, 2023, **13**, 2632–2656; (*b*) S. H. Park, N. Kwon, J. H. Lee, J. Yoon and I. Shin, *Chem. Soc. Rev.*, 2020, **49**, 143–179.
12 (*a*) C. Zhao, S. Hussain, J. Li, C. Liu, M. A. Afroz, C. Zhu, Z. Yue, J. Zhang, Y. Hao and R. Gao, *Anal. Chem.*, 2025, **97**, 10027–10037; (*b*) X. Chen, S. Hussain, Y. Tang, X. Chen, S. Zhang, Y. Wang, P. Zhang, R. Gao, S. Wang and Y. Hao, *Sci. Total Environ.*, 2023, **860**, 160467.
13 R. F. Menger, E. Funk, C. S. Henry and T. Borch, *Chem. Eng. J.*, 2021, **417**, 129133.
14 (*a*) C. Nie, J. Shui, L. Huang, J. Wang, Y. Shen and Y. Wu, *Anal. Chem.*, 2024, **96**, 13512–13521; (*b*) J. Park, K. A. Yang, Y. Choi and J. K. Choe, *Environ. Int.*, 2022, **158**, 107000.
15 (*a*) K. N. Kang and Y. S. Lee, *Future Trends in Biotechnology*, ed. J. J. Zhong, Springer, Berlin, 2013, pp. 153–169; (*b*) H. Xing, K. Hwang, J. Li, S. F. Torabi and Y. Lu, *Curr. Opin. Chem. Eng.*, 2014, **4**, 79–87.
16 (*a*) B. S. Gaylord, A. J. Heeger and G. C. Bazan, *J. Am. Chem. Soc.*, 2003, **125**, 896–900; (*b*) Y. Zhou, J. Zhang, L. Zhao, Y. Li, H. Chen, S. Li and Y. Cheng, *ACS Appl. Mater. Interfaces*, 2016, **8**, 1520–1526; (*c*) Z. Zhang, X. Xia, X. Xiang, F. Huang and L. Han, *Sens. Actuators, B*, 2017, **249**, 8–13; (*d*) Y. Liu, S. Meng, J. Qin, R. Zhang, N. He, Y. Jiang, H. Chen, N. Li and Y. Zhao, *Int. J. Biol. Macromol.*, 2022, **219**, 346–352.
17 (*a*) R. Salimian and C. Nardin, *Biomacromolecules*, 2023, **24**, 3411–3437; (*b*) Y. Liu, H. Yan, J. Shangguan, X. Yang, M. Wang and W. Liu, *Microchim. Acta*, 2018, **185**, 427; (*c*) X. Liu, X. Hua, Q. Fan, J. Chao, S. Su, Y. Q. Huang, L. Wang and W. Huang, *ACS Appl. Mater. Interfaces*, 2015, **7**, 16458–16465; (*d*) P. Zhang, K. Qin, A. Lopez, Z. Li and J. Liu, *Anal. Chem.*, 2022, **94**, 15456–15463.
18 (*a*) Z. Jing, R. Li, J. Zhao, R. Yuan and S. Chen, *Anal. Chem.*, 2024, **96**, 18178–18186; (*b*) W. Yao, X. Xu, X. Zhai, T. Ji, R. Zhang, S. Xu and X. Luo, *Angew. Chem., Int. Ed.*, 2025, e16838.
19 F. He, Y. Tang, S. Wang, Y. Li and D. Zhu, *J. Am. Chem. Soc.*, 2005, **127**, 12343–12346.

20 X. J. Xing, X. G. Liu, Y. He, Y. Lin, C. L. Zhang, H. W. Tang and D. W. Pang, *Biomacromolecules*, 2013, **14**, 117–123.
21 J. Mao, Y. Zhang, S. Zhang and B. Song, *Langmuir*, 2024, **40**, 5479–5487.
22 K. Tkacz, M. Modzelewska-Kapituła, A. Więk and Z. Nogalski, *Appl. Sci.*, 2020, **10**, 8215.
23 Q. Chen, P. Zhu, J. Xiong, L. Gao and K. Tan, *Spectrochim. Acta, Part A*, 2020, **224**, 117362.